Conversion of bright magneto-optical resonances into dark resonances at fixed laser frequency for D_2 excitation of atomic rubidium

M. Auzinsh,* A. Berzins, R. Ferber, F. Gahbauer, L. Kalvans, A. Mozers, and D. Opalevs
Laser Centre, The University of Latvia, LV-1586 Riga, Latvia
(Received 29 November 2011; published 16 March 2012)

Nonlinear magneto-optical resonances on the hyperfine transitions belonging to the D_2 line of rubidium were changed from bright to dark resonances by changing the laser power density of the single exciting laser field or by changing the vapor temperature in the cell. In one set of experiments atoms were excited by linearly polarized light from an extended cavity diode laser with polarization vector perpendicular to the light's propagation direction and magnetic field, and laser-induced fluorescence was observed along the direction of the magnetic field, which was scanned. A low-contrast bright resonance was observed at low laser power densities when the laser was tuned to the $F_g = 2 \longrightarrow F_e = 3$ transition of ^{87}Rb and near to the $F_g = 3 \longrightarrow F_e = 4$ transition of ^{85}Rb. The bright resonance became dark as the laser power density was increased above 0.6 mW/cm^2 or 0.8 mW/cm^2, respectively. When the $F_g = 2 \longrightarrow F_e = 3$ transition of ^{87}Rb was excited with circularly polarized light in a second set of experiments, a bright resonance was observed, which became dark when the temperature was increased to around 50 °C. The experimental observations at room temperature could be reproduced with good agreement by calculations based on a theoretical model, although the theoretical model was not able to describe measurements at elevated temperatures, where reabsorption was thought to play a decisive role. The model was derived from the optical Bloch equations and included all nearby hyperfine components, averaging over the Doppler profile, mixing of magnetic sublevels in the external magnetic field, and a treatment of the coherence properties of the exciting radiation field.

DOI: 10.1103/PhysRevA.85.033418 PACS number(s): 32.80.Xx, 42.50.Gy, 32.60.+i

I. INTRODUCTION

Coherences between atomic states can be exploited to modify the optical properties of a medium, which is usually an atomic vapor [1] but may also be a solid-state system [2] or an artificial atom [3]. In the phenomenon of electromagnetically induced transparency (EIT), one uses two lasers in a Λ configuration to create a coherent superposition of the two lower states that is nonabsorbing or dark [4,5]. Instead of using two laser fields and their relative detuning to create the dark coherent superposition, it is possible to create the Λ system with the two orthogonally circularly polarized components of a single, linearly polarized laser field and a ground state with degenerate magnetic sublevels. In this case, one speaks of a dark nonlinear magneto-optical resonance [6], and the coherent superposition is created or destroyed by applying a magnetic field that shifts the energies of the magnetic sublevels of a ground state with nonzero angular momentum. It is also possible to create coherent superposition states with enhanced absorption, in which case one has electromagnetically induced absorption (EIA) [7] and the related bright, nonlinear magneto-optical resonances [8] are observed. Recently, attention has been focused on the conversion of EIT to EIA as a function of the properties of the pump field, such as polarization [9] and laser power density [10–13]. In this work we investigate the conversion of a bright, nonlinear magneto-optical resonance to a dark resonance with a single laser field at fixed frequency as a function of laser power density.

A number of interesting experiments and theoretical studies have been reported recently for EIT and EIA with two light fields in the Hanle configuration. In the Hanle configuration, two atomic states are coupled in a Λ or V scheme whose legs are formed by coherent light fields of orthogonal circular polarization (see, for example, Ref. [6]). Sign changes in EIA and EIT spectra were observed on a beam of cesium atoms with copropagating pump and probe beams of various polarizations [11,14]. In this case the Doppler effect was minimal because of the atomic beam. Copropagating pump and probe beams also were used to change EIT to EIA as a function of pump intensity on the $F_g = 2 \longrightarrow F_e = 3$ transition of the D_2 line of rubidium [13]. Theoretical calculations on an analogous system of lower angular momentum were used to argue that the effect was not due to Doppler broadening but rather by population shifts caused by the two competing laser fields. However, experimental and theoretical curves could not be compared directly as the angular momentum was not the same. Similar changes from EIA to EIT were observed in the case of two counterpropagating laser fields of opposite circular polarization (Hanle configuration) from a single laser on the $F_g = 2 \longrightarrow F_e = 3$ transition of the D_2 line of ^{87}Rb [12]. Again, detailed theoretical calculations supported the conclusion that the change from EIA to EIT in the forward field were caused by the competing action of the two laser fields on the population of magnetic sublevels. However, the theoretical calculation was not done for the precise angular-momentum states studied in the experiment, and, hence, experimental and theoretical curves could not be directly compared. Interestingly, a dip in transmission was observed with linearly polarized excitation in the absence of a probe field. Our results show that changes from dips to peaks in absorption can be achieved with a single laser field in an atomic vapor, when changes in the intensity of the exciting laser radiation influence the competition between

*marcis.auzins@lu.lv

two neighboring levels and also between the polarization components of a single level. We demonstrate the ability of computational models to describe these effects in detail by directly comparing experimental and theoretical curves.

Dark, nonlinear magneto-optical resonances have been known for a long time [15] and studied in great detail. Bright resonances attracted attention [8] and were explained [16,17] more recently. For linearly polarized exciting radiation, bright resonances can appear when the total angular momentum of the excited state F_e is greater than the total angular momentum of the ground state F_g. Unlike dark resonances, in which a coherent dark state is formed, bright resonances occur when atomic populations are redistributed by various excitation and relaxation cycles into states that interact more strongly with the exciting radiation. Thus, bright resonance contrast on open transitions, if observable at all, is very small. Observing bright resonances is complicated by the fact that in most alkali-metal systems, the excited state hyperfine structure (HFS) is only partially resolved under Doppler broadening. Thus, even when the laser is tuned to a bright resonance, neighboring dark resonances can be excited in atoms belonging to different velocity groups. The extent to which neighboring transitions are excited can also depend on power broadening of the laser. A further complication arises from the fact that some hyperfine transitions are cycling, while others are partially open. In the case of cycling transitions, atoms are redistributed among different coherent atomic states of the same hyperfine level according to the respective transitions strengths. In partially open transitions, population can be lost to other hyperfine levels. In any case, the intensity of the exciting laser must be taken into account. As a result, in order to make realistic comparisons between experiment and theory, it is important to have a good model that takes into account the finite laser linewidth, Doppler broadening and power broadening, and the nonlinear Zeeman splitting with the mixing of magnetic sublevels in the magnetic field.

In the experimental conditions studied here, the problem is highly nonlinear and it is not possible to give a complete description with analytical models. Numerical models based on the optical Bloch equations were developed, first, for atomic beams [18], in which Doppler broadening is minimal. In time, such models were expanded to include Doppler broadening and neighboring hyperfine transitions [19], but a detailed treatment of the coherence properties of the laser radiation was not included. When the coherence properties of the laser radiation were included [20,21], along with averaging over the Doppler profile, good agreement between theoretical and experimental signals for nonlinear magneto-optical resonances could be achieved, for example, for D_1 excitation in cesium [22] and rubidium [23]. D_2 excitation in rubidium presents an additional challenge, because the hyperfine splitting of the excited state is smaller relative to the Doppler broadening than in the case of D_1, and so neighboring states influence more strongly.

In this work, we report that when a single, linearly polarized laser field was tuned to the $F_g = 2 \longrightarrow F_e = 3$ transition of ^{87}Rb and the $F_g = 3 \longrightarrow F_e = 4$ transition of ^{85}Rb, bright resonances became dark when the laser power density was increased. Experimental measurements were reproduced by theoretical calculations conducted for the same transition that was measured. The sensitivity of the resonances' shapes to the experimental parameters provided a stringent test of the theoretical model. As an additional example of a resonance that changes sign for fixed laser frequency and as stimulus for further study, we also present measurements of a fluorescence maximum that becomes a minimum as the temperature is increased for circularly polarized excitation of the $F_g = 2 \longrightarrow F_e = 3$ transition of ^{87}Rb.

II. EXPERIMENTAL DESCRIPTION

Figure 1 shows the level scheme of the D_2 line of rubidium. Note that the hyperfine transitions of the excited state of the ^{85}Rb D_2 line are essentially unresolved under the typical Doppler broadening at room temperature, which has a full width at half maximum (FWHM) of approximately 500 MHz, while they are partially resolved in the case of ^{87}Rb.

The geometry of the excitation in the experiment is given in Fig. 2. The exciting laser radiation was linearly polarized with polarization vector perpendicular to the magnetic field and to the propagation direction of the radiation. For some experiments, a Thorlabs achromatic $\lambda/4$ plate was inserted after the linear polarizer to produce circularly polarized radiation in the cell. The observation direction was parallel to the magnetic field.

The laser was an external cavity diode laser. The temperature of the box and the diode were stabilized by Thorlabs TED200 temperature controllers, and the current was controlled by a Thorlabs LDC205B current controller. The laser frequency was stabilized manually, and the frequency drift during a typical data-taking run was typically around 10 MHz or less. The wavelength was monitored by a HighFinesse WS-7 wavemeter. A Thorlabs BP104-VIS beam profiler was used to measure the beam diameter, which was taken to be the FWHM of the intensity distribution. The cell was a 25-mm-long pyrex cell with optical quality windows filled with natural rubidium and produced by Toptica, A.G. The laser radiation entered the cell through a Glan-Thompson polarizer. A combination

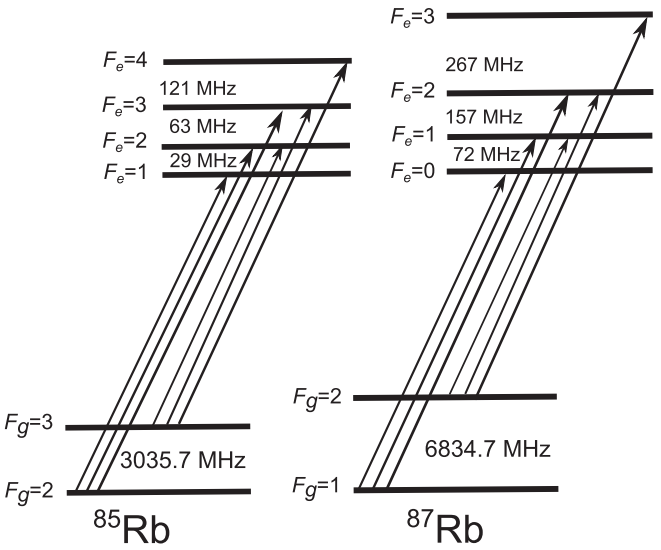

FIG. 1. Hyperfine level structure and transitions of the D_2 line of rubidium.

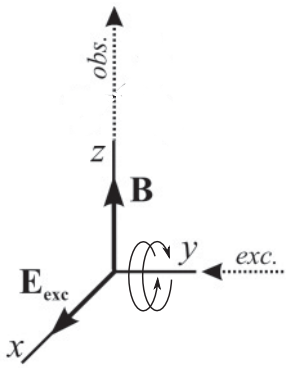

FIG. 2. Experimental geometry. The relative orientation of the laser beam (*exc*), laser light polarization ($\mathbf{E}_{\rm exc}$), magnetic field ($\mathbf{B}$), and observation direction (*obs*). Circularly polarized light could be produced by means of a $\lambda/4$ plate.

of neutral density filters and a polarization rotator before the polarizer was used to select various laser power densities. The laser-induced fluorescence (LIF) was focused onto a Thorlabs FDS100 photodiode and amplified. Signals were recorded by an Agilent DSO5014A oscilloscope.

The cell was located at the center of a three-axis Helmholtz coil. Two coils were used to compensate the ambient magnetic field. The residual magnetic field was estimated to be less than 10 mG. The third coil was used to scan the magnetic field along the z axis as indicated in Fig. 2 using a bipolar BOP-50-8-M power supply from Kepco. In order to find the appropriate current for the field compensation, the polarization vector of the laser beam was rotated parallel to the z axis and the magnetic field was scanned along the z axis while the current in the compensating coils was adjusted in order to eliminate the magneto-optical resonance that appears when the field is not compensated. The cell was at room temperature, except for those experiments that investigated the temperature dependence, when the cell was heated with hot air. The air was heated some distance away from the cell to avoid stray magnetic fields from the heating currents. The temperature was measured with two thermocouples near the cell, though the thermocouples were removed during the measurements as they were slightly magnetized.

III. THEORETICAL MODEL

The atomic state was described by a density matrix ρ in the ξ, F, m_F basis, where F denotes the total atomic angular-momentum quantum number (that characterizes the hyperfine structure), m_F labels the respective magnetic quantum number for Zeeman splitting, and ξ represents all other quantum numbers. The fluorescence signal can be calculated from the part of the density matrix that describes the population and Zeeman coherences of the excited state $\rho_{e_i e_j}$. To do so, the optical Bloch equations (OBEs) that describe the time evolution of a density matrix were employed [24]:

$$i\hbar\frac{\partial\rho}{\partial t} = [\hat{H},\rho] + i\hbar\hat{R}\rho. \tag{1}$$

We assumed that the interaction between the atoms and the exciting field was described in the dipole approximation by the interaction operator $\hat{V} = -\hat{\mathbf{d}}\cdot\mathbf{E}(t)$. The electric field $\mathbf{E}(t)$ was treated as a classically oscillating field with a stochastically fluctuating phase. As the energy shifts due to the magnetic field were small compared to the fine-structure splitting, the Hamiltonian of the atomic interaction with the magnetic field could be written as

$$\hat{H}_B = \frac{\mu_B}{\hbar}(g_J\mathbf{J} + g_I\mathbf{I})\cdot\mathbf{B}, \tag{2}$$

and expanded as shown, for example, in Ref. [25]. We denote the unperturbed atomic Hamiltonian as $\hat{H}_0$, and so the full Hamiltonian of the system is

$$\hat{H} = \hat{H}_0 + \hat{H}_B + \hat{V}. \tag{3}$$

The relaxation operator $\hat{R}$ in Eq. (1) consists of the spontaneous emission rate, equal to the natural linewidth Γ of the transition and the transit relaxation rate γ, which comes about because the moving atoms spend a finite time in the laser beam. The rate of atom-atom collisions in our experimental conditions (vacuum cell at room temperature) were estimated to be at least two orders of magnitude less than the transit relaxation rate and, therefore, were neglected.

The OBEs [Eq. (1)] were treated to obtain rate equations for the Zeeman coherences of the ground and excited states. The treatment included the rotating-wave approximation [26], averaging and decorrelation of the stochastic phase [27], and adiabatic elimination of the optical coherences (see Ref. [21] for details). As a result, the following rate equations were obtained:

$$\begin{aligned}\frac{\partial\rho_{g_i g_j}}{\partial t} &= \left(\Xi_{g_i e_m} + \Xi^*_{e_k g_j}\right)\sum_{e_k,e_m} d^*_{g_i e_k} d_{e_m g_j}\rho_{e_k e_m} \\ &\quad - \sum_{e_k,g_m}\left(\Xi^*_{e_k g_j} d^*_{g_i e_k} d_{e_k g_m}\rho_{g_m g_j} + \Xi_{g_i e_k} d^*_{g_m e_k} d_{e_k g_j}\rho_{g_i g_m}\right) \\ &\quad - i\omega_{g_i g_j}\rho_{g_i g_j} - \gamma\rho_{g_i g_j} + \sum_{e_k e_l}\Gamma^{e_k e_l}_{g_i g_j}\rho_{e_k e_l} + \lambda\delta(g_i,g_j)\end{aligned} \tag{4a}$$

$$\begin{aligned}\frac{\partial\rho_{e_i e_j}}{\partial t} &= \left(\Xi^*_{e_i g_m} + \Xi_{g_k e_j}\right)\sum_{g_k,g_m} d_{e_i g_k} d^*_{g_m e_j}\rho_{g_k g_m} \\ &\quad - \sum_{g_k,e_m}\left(\Xi_{g_k e_j} d_{e_i g_k} d^*_{g_k e_m}\rho_{e_m e_j} + \Xi^*_{e_i g_k} d_{e_m g_k} d^*_{g_k e_j}\rho_{e_i e_m}\right) \\ &\quad - i\omega_{e_i e_j}\rho_{e_i e_j} - (\Gamma+\gamma)\rho_{e_i e_j}.\end{aligned} \tag{4b}$$

In Eq. (4) the Zeeman coherences of the ground and excited states are denoted by $\rho_{g_i g_j}$ and $\rho_{e_i e_j}$, respectively. Each term of the rate equations describes a well-defined part of the atom-light interaction process. Thus, the first terms in both Eqs. (4a) and (4b) describe the population increase and the creation of Zeeman coherences, and the second terms denote the population decrease and the destruction of Zeeman coherences in the respective atomic state (ground or excited) due to the laser-induced transitions; $d_{e_i g_j}$ is the dipole transition matrix element between the ground state i and the excited state j [28], while $\Xi_{e_i g_j}$ describes the rate of the atomic transitions induced by the exciting radiation and is defined below [Eq. (5)]. The third term of Eqs. (4) describes the

destruction of the Zeeman coherences by the external magnetic field; ω_{ij} is the splitting of the Zeeman sublevels. The fourth term describes the relaxation processes, and the fifth and sixth [absent in Eq. (4b)] describe the repopulation of the ground state due to spontaneous transitions and "fresh" atoms flying into the region of the interaction. It was assumed that the atomic equilibrium density outside the interaction region is normalized to unity, and so $\lambda = \gamma$. The transit relaxation rate was used as an adjustable parameter and corresponds to the average time spent by the atoms in the interaction region.

The interaction strength $\Xi_{e_i g_j}$ is given by

$$\Xi_{e_i g_j} = \frac{|\varepsilon_{\bar{\omega}}|^2}{\hbar^2} \frac{1}{\frac{\Gamma+\gamma+\Delta\omega}{2} + i(\bar{\omega} - \mathbf{k}_{\bar{\omega}} \cdot \mathbf{v} - \omega_{e_i g_j})}, \tag{5}$$

where $\Delta\omega$ is the linewidth of the exciting radiation of central frequency $\bar{\omega}$ and $\mathbf{k}_{\bar{\omega}} \cdot \mathbf{v}$ is the frequency shift due to the Doppler effect. The value $\frac{|\varepsilon_{\bar{\omega}}|}{\hbar}$ is proportional to the Rabi frequency, which describes the coupling strength induced by the oscillating electric field between the chosen atomic states as follows:

$$\Omega_R^2 = \frac{|\varepsilon_{\bar{\omega}}|^2}{\hbar^2} \|d\|^2, \tag{6}$$

where $\|d\|$ is the reduced dipole transition matrix element, which is equal for all d_{ij} elements in Eqs. (4). The Rabi frequency squared is proportional to the exciting radiation's power density with some proportionality coefficient k_{Rabi},

$$I = k_{\text{Rabi}} \Omega_R^2, \tag{7}$$

and it is used as an adjustable parameter that corresponds to the exciting radiation's power density.

The experiments took place under stationary excitation conditions, for which Eqs. (4) are valid. Thus, $\frac{\partial \rho_{g_i g_j}}{\partial t} = \frac{\partial \rho_{e_i e_j}}{\partial t} = 0$, and the differential equations [Eqs. (4)] were reduced to a system of linear equations that could be solved to obtain the density matrix components that describe the Zeeman coherences of both the atomic ground and excited states. From the obtained density matrix, the fluorescence signal was calculated as

$$I_{fl}(\vec{e}) = \tilde{I}_0 \sum_{g_i, e_j, e_k} d^{(ob)*}_{g_i e_j} d^{(ob)}_{e_k g_i} \rho_{e_j e_k}, \tag{8}$$

where $\tilde{I}_0$ is a constant of proportionality and $d^{(ob)}_{ij}$ is the matrix element of the dipole transition at the observation geometry.

A summation over the different atomic velocity groups, associated to different $\mathbf{v}$ in Eq. (5), was performed to describe the Doppler broadening of the transitions. When the density matrix and the fluorescence signal were calculated, we took into account all nearby hyperfine transitions of both the ground and the excited states, represented by different $w_{e_i g_j}$ in Eq. (5). Atomic constants were taken from Refs. [25,29]. Some parameters could not be determined directly with certainty. Starting from reasonable estimates, these parameter values were varied in different sets of simulations in order to find the set of parameters that provided the best overall agreement between experiment and theory. We required the parameter values to be consistent for all measurements, even if the agreement between theory and experiment for individual cases was not the best that could have been achieved by tailoring the parameters for each case. Thus, the laser linewidth was assumed to be $\Delta\omega = 2$ MHz. The proportionality constant k_{Rabi} between the laser power density I and the square of the Rabi frequency Ω ($I = k_{\text{Rabi}}\Omega^2$) was $k_{\text{Rabi}} = 0.575$, with the Rabi frequency given in MHz and the laser power density in mW/cm^2. The relationship between the transit relaxation rate γ and the laser beam diameter d was $\gamma = 0.0033/d$ with the transit relaxation rate in MHz and the laser beam diameter in cm. The standard deviation of the Doppler profile was assumed to be 216 MHz, and it was sampled with a step size of less than 2 MHz during the averaging over the Doppler distribution. No additional background was subtracted beyond the background determined during the experiment by blocking the laser beam.

IV. RESULTS AND DISCUSSION

The fluorescence signals recorded as a function of magnetic field usually showed two kinds of structure. One structure was broad, with a width on the order of several gauss. This structure was caused by coherences in the excited state as well as by Zeeman sublevels being shifted out of resonance with the laser. The broad structure also tended to have a strong contrast, on the order of several percent or even tens of percent. In addition to the broad structure, it was also possible to observe narrow features, centered around zero magnetic field, with widths on the order of several hundred milligauss. These resonances were related to the destruction of coherences in the ground state as a magnetic field breaks the degeneracy of the magnetic sublevels. The features were also very small, with contrasts from a fraction of a percent to a few percent. (We defined the contrast of the narrow structure with respect to the estimated zero-field value of the curve corresponding to the larger structure.) Our study was focused on these narrow resonances and the way their contrast and even their sign depended on the laser power density and temperature. Thus, in the results that follow, only a narrow range of the magnetic field is shown.

Figure 3 shows the LIF intensity as a function of magnetic field for various values of the power density of the exciting laser radiation with the laser tuned to the $F_g = 2 \longrightarrow F_e = 3$ transition of ^{87}Rb. The laser beam diameter was 2.1 mm. This transition could be expected to be bright because $F_g < F_e$. Indeed, a very weak bright resonance with contrast on the order of 0.3% was observed when the laser power density was 0.14 mW/cm^2. However, as the power density of the exciting laser radiation was increased, the bright resonance disappeared and became dark for laser power densities greater than about 0.6 mW/cm^2. At a laser power density of 2.9 mW/cm^2, the contrast of the dark resonance with respect to the intensity at the inflection point of the larger structure was about 2%. The resonances appeared to be somewhat narrower in the calculations than in the experiment. The reason for this discrepancy was most likely a residual transverse magnetic field on the order of a few milligauss. It should also be pointed out that the model made the simplifying assumption that the laser power density was constant over the laser beam width, whereas in reality there was a distribution of laser power densities. Nevertheless, given the subtle nature of the effect, the agreement between experiment and theory was acceptable.

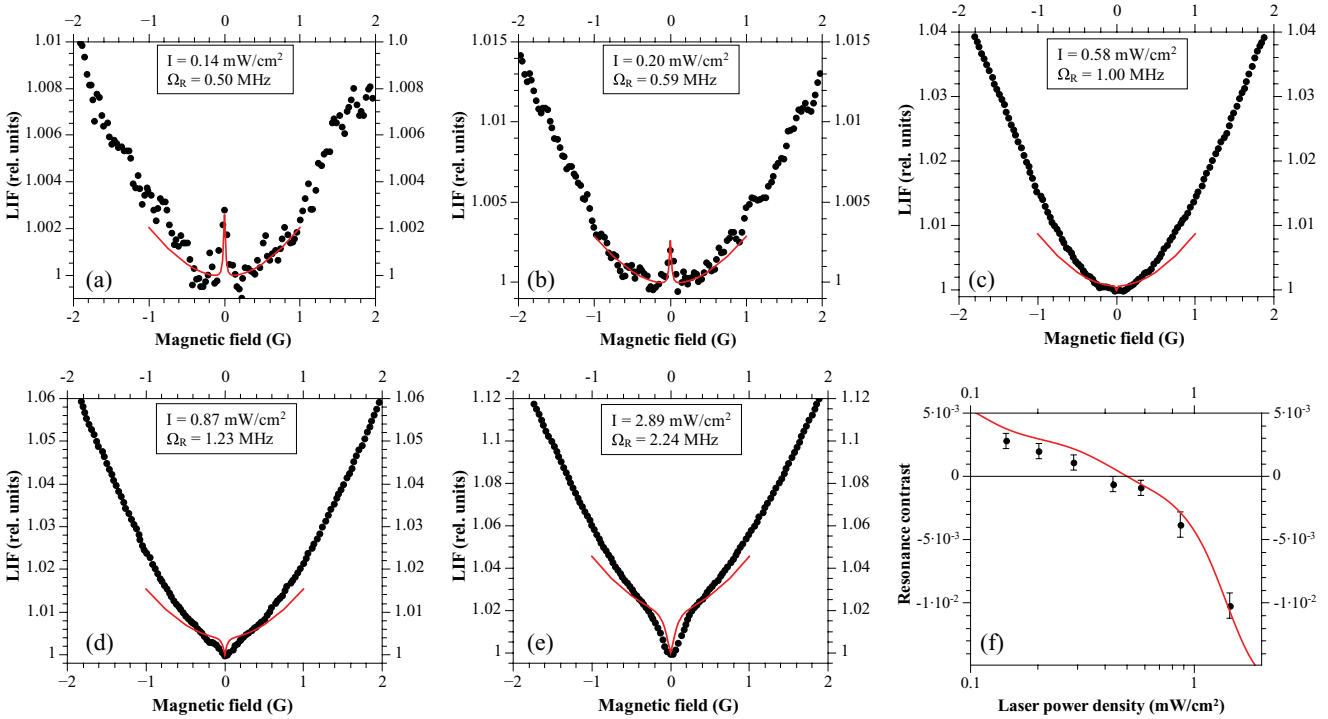

FIG. 3. (Color online) Bright and dark resonances for various laser-power densities with the laser tuned to the $F_g = 2 \longrightarrow F_e = 3$ transition of ^{87}Rb for linearly polarized exciting laser radiation with a beam diameter of 2.1 mm. Markers represent the experimental results, whereas the solid line represents the results of calculations. The final panel shows the contrast of the narrow resonance referenced to the estimated background due to the broad structure at zero magnetic field.

The theoretical model unambiguously reproduced the change from a bright to a dark resonance for laser power densities above $I = 0.4$ mW/cm^2. In order to understand the effect qualitatively, one must keep in mind that Doppler broadening allows the laser to excite the neighboring $F_g = 2 \longrightarrow F_e = 2$ transition, and so the observed signal is the result of a superposition of the bright resonance at the $F_g = 2 \longrightarrow F_e = 3$ transition and the dark resonance at the $F_g = 2 \longrightarrow F_e = 2$ transition. Figure 4 shows the calculated contrasts as a function of laser power density for laser radiation in resonance with each of these two transitions

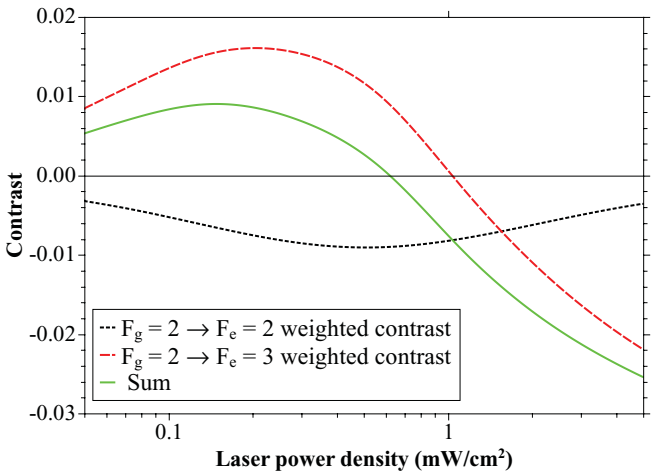

FIG. 4. (Color online) Calculated contrasts as a function of laser power density of the resonances at the $F_g = 2 \longrightarrow F_e = 2$ and $F_g = 2 \longrightarrow F_e = 3$ transitions of ^{87}Rb weighted by the relative number of atoms in the velocity group that is in resonance with a laser tuned to the $F_g = 2 \longrightarrow F_e = 3$ transition.

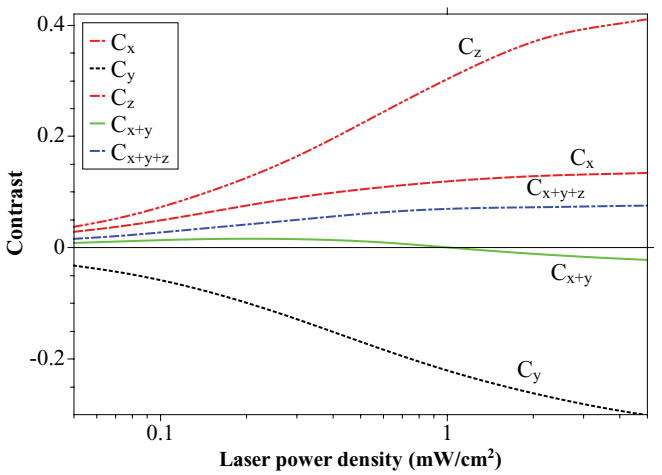

FIG. 5. (Color online) Contrast as a function of laser power density of the resonance at the $F_g = 2 \longrightarrow F_e = 3$ transition of ^{87}Rb when particular polarization components of the fluorescence intensity I are observed. The curves give the contrasts C_x, C_y, C_z, C_{x+y}, and C_{x+y+z} for the three orthogonal polarization components of the fluorescence I_x, I_y, and I_z, as well as for the components I_{x+y} and I_{x+y+z}. The calculations were performed without taking into account the Doppler effect. Note that the contrast is a relative figure, whereas the intensities I_x, I_y, and I_z differ in their dependence on laser power density and magnetic field. Note also that the solid green line represents the same quantity as the solid green line in Fig. 4.

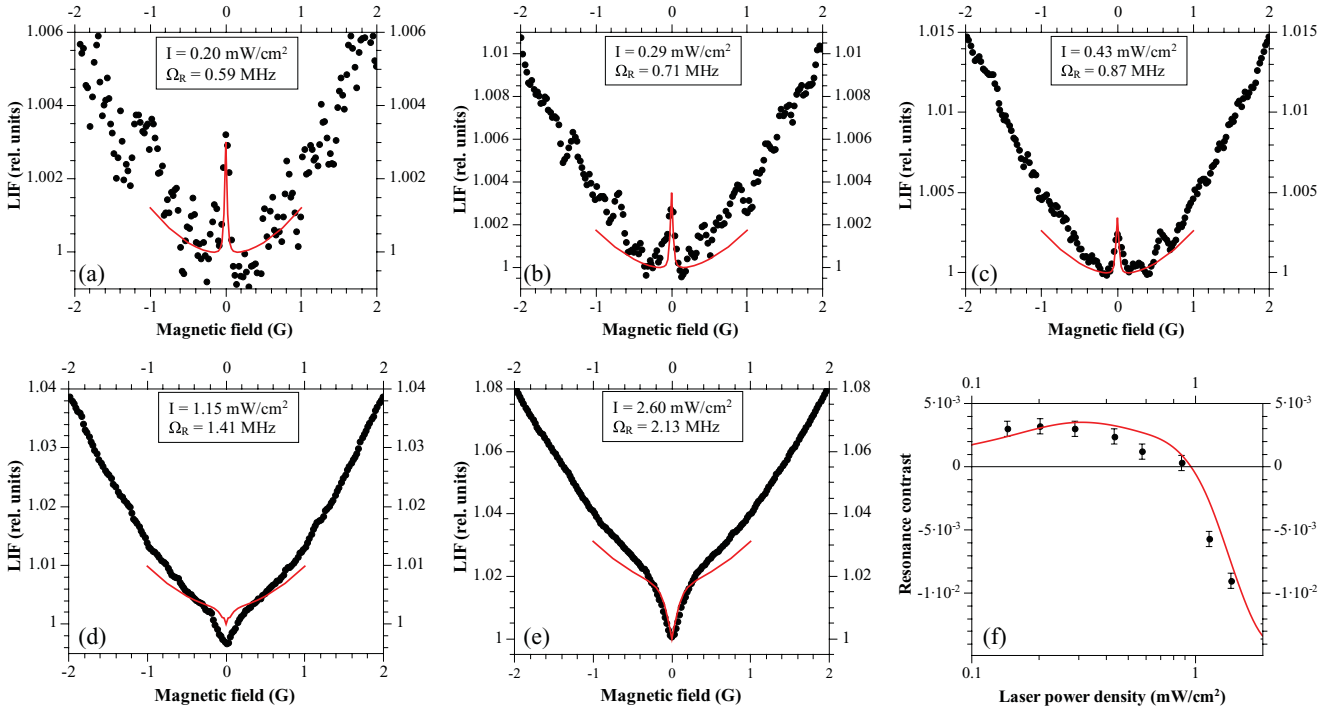

FIG. 6. (Color online) Bright and dark resonances obtained at various laser power densities near the $F_g = 3 \longrightarrow F_e = 4$ transition of ^{85}Rb. The laser was detuned from the exact transition by 200 MHz in the direction away from the $F_g = 3 \longrightarrow F_e = 4$ transition for linearly polarized exciting laser radiation with a beam diameter of 2.1 mm. Markers represent the experimental results, whereas the solid line represents the results of calculations. The final panel shows the contrast of the narrow resonance referenced to the estimated background due to the broad structure at zero magnetic field.

but ignoring Doppler broadening. The curves in that figure suggest that the bright resonance at the $F_g = 2 \longrightarrow F_e = 3$ transition would become dark in any case for laser power densities above a few mW/cm^2, even without the influence of the neighboring transition. There is no reason why a bright resonance should become dark merely because of a change in laser-power density. However, while a resonance that includes the total fluorescence must remain bright, different polarization components of this fluorescence may behave differently, and in the experiment not all polarization components were observed. Figure 5 shows the calculated contrast of resonances observed for each of three orthogonally polarized fluorescence components: the x and z components

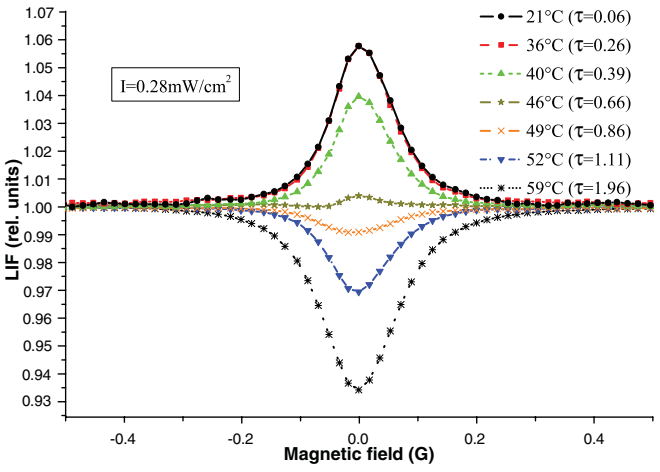

FIG. 7. (Color online) Dark and bright resonances obtained at various vapor temperatures at the $F_g = 2 \longrightarrow F_e = 3$ transition of ^{87}Rb for circularly polarized excitation at a laser-power density of around 0.28 mW/cm^2. Experimental measurements are shown. The optical depth τ along the laser beam inside the cell is given in parentheses next to the temperature. The curves for 21 °C and 36 °C overlap.

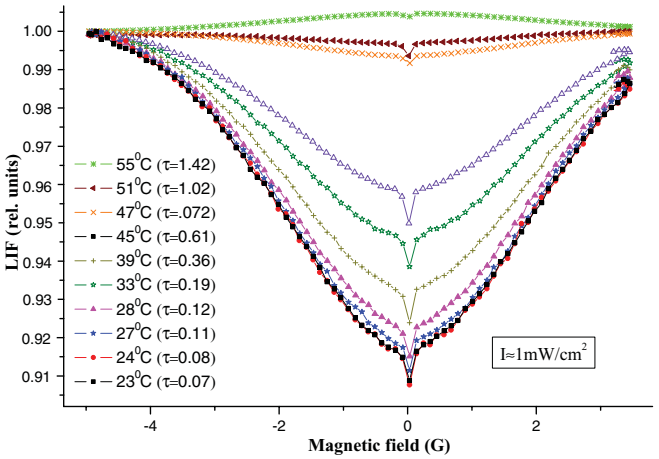

FIG. 8. (Color online) Dark resonances obtained at various vapor temperatures at the $F_g = 2 \longrightarrow F_e = 3$ transition of ^{87}Rb for linearly polarized excitation at a laser power density of around 1 mW/cm^2. Experimental measurements are shown. The optical depth τ along the laser beam inside the cell is given in parentheses next to the temperature.

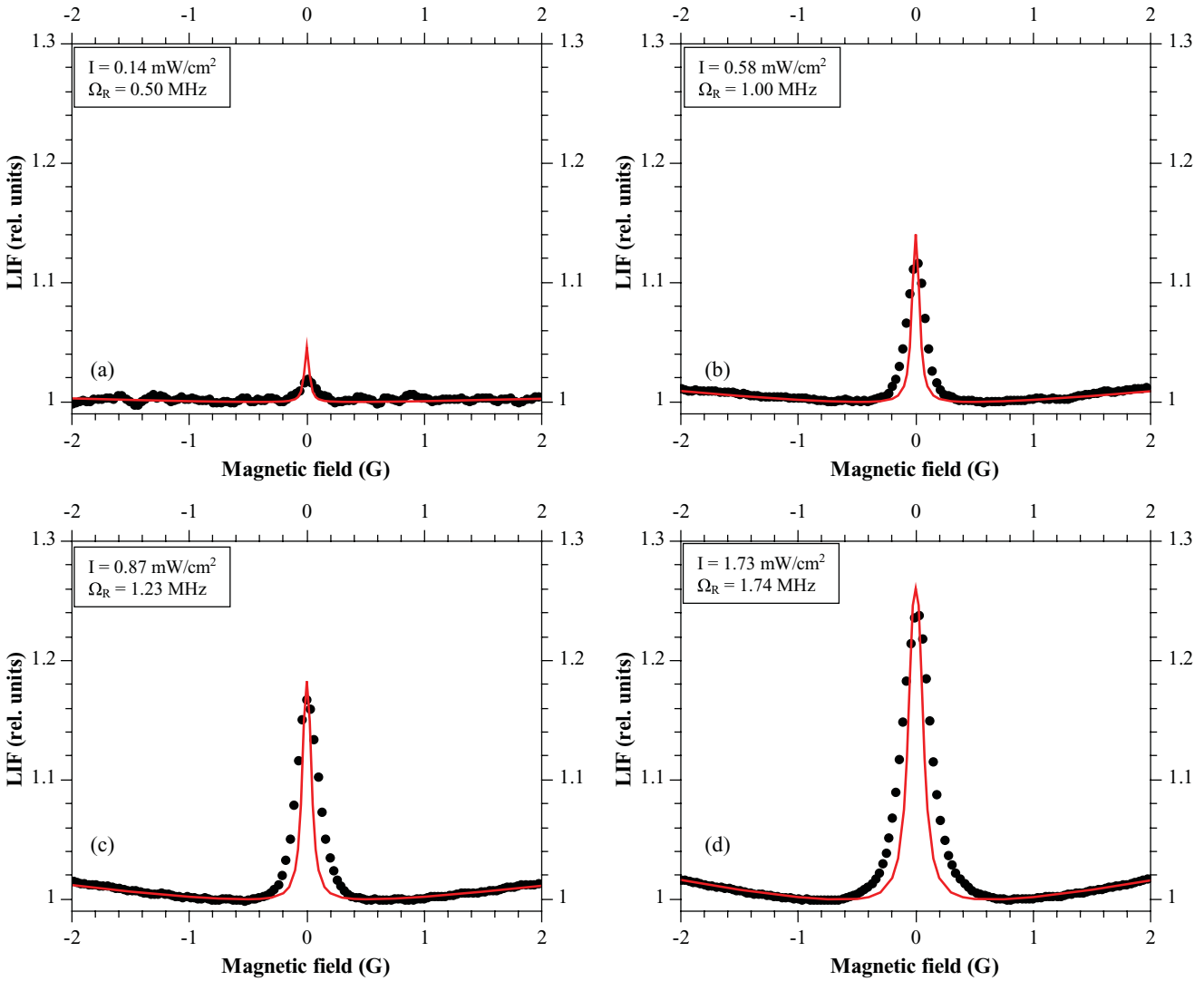

FIG. 9. (Color online) Bright resonances obtained at various laser power densities for circularly polarized excitation of the $F_g = 2 \longrightarrow F_e = 3$ transition of ^{87}Rb. Markers represent the experimental results, whereas the solid line represents the results of calculations.

always give a bright resonance, while the y component is always dark. In our observation geometry we registered the x and y components, and, as can be seen in the figure, the contrast of the "dark" y component changes more rapidly. When the contrasts are weighted by the actual fluorescence intensities, the y component actually becomes dominant at larger excitation power densities. Nevertheless, in the total fluorescence emitted in all directions (labelled C_{x+y+z} in Fig. 5) a bright resonance still would be observed. In other words, at each value of the magnetic field, the degree of polarization is a function of laser power density, and, in a particular observation geometry, this dependence can change the contrast of a resonance from bright to dark.

Figure 6 shows magneto-optical resonances obtained near the $F_g = 3 \longrightarrow F_e = 4$ transition of ^{85}Rb but with the laser detuned by 200 MHz in the direction away from the $F_g = 3 \longrightarrow F_e = 3$ transition. A bright resonance was observed at very low laser power densities. Similarly to the case of the $F_g = 2 \longrightarrow F_e = 3$ transition of ^{87}Rb, the resonance became dark for laser power densities greater than 0.8 mW/cm^2. When the laser was tuned directly to the $F_g = 3 \longrightarrow F_e = 4$ transition of ^{85}Rb, no bright resonance was observed even for laser power densities as low as 0.14 mW/cm^2. The reason was probably the influence of the strong dark resonance at the nearby $F_g = 3 \longrightarrow F_e = 3$ transition, which could be excited for some velocity groups of atoms. Power broadening may also have played a small role in exciting this nearby transition. Even if the $F_g = 3 \longrightarrow F_e = 3$ transition was excited only weakly, it could easily overwhelm the bright resonance at the $F_g = 3 \longrightarrow F_e = 4$ transition. The laser beam diameter for this series of measurements was 2.1 mm.

Figure 7 shows the fluorescence signals obtained at the $F_g = 2 \longrightarrow F_e = 3$ transition of ^{87}Rb at various vapor temperatures and for circularly polarized excitation. The elevated temperatures were achieved by conducting hot air around the cell as described in Sec. II. As the temperature was increased, the contrast of the bright resonance decreased until the bright resonance disappeared at around 40 °C. At this temperature, the optical depth traversed by the laser beam in the 25-mm-long cell was ~0.39. At higher temperatures, a dark resonance was

observed, and its contrast grew with increasing temperature. The change from bright to dark resonance around an optical depth of 0.66 was probably related to reabsorption. With each reabsorption cycle, information about the original coherent atomic state is lost. This hypothesis is supported by the fact that the optical depth at which the bright resonance disappeared ($\sim$0.66) roughly corresponded to the optical depth at which the ratio of the incoherent pumping rate to other relaxation rates reaches 1.5 and continues to increase (see Ref. [30], Fig. 5). Similar measurements were made for linearly polarized light (see Fig. 8). In that case, although the contrast of the dark resonance decreased with temperature, it never changed sign. The case of circularly polarized light had been studied earlier in the context of CPT resonances, and a similar change in resonance sign with temperature had been observed [31].

Our theoretical model did not include effects that become important at elevated temperatures, such as reabsorption. Thus, the change from bright to dark of the resonance at the $F_g = 2 \longrightarrow F_e = 3$ transition of ^{87}Rb excited by circularly polarized light could not be reproduced by our model. Nevertheless, the model could be checked against the results at room temperature.

Figure 9 shows measured and calculated signals for bright resonances obtained by exciting the $F_g = 2 \longrightarrow F_e = 3$ transition of ^{87}Rb with circularly polarized laser radiation at various laser power densities. The rubidium vapor was at room temperature. The change in temperature was accompanied by a change from bright to dark resonance with contrasts on the order of 6%, much larger than in the case of linearly polarized excitation. The theoretical calculations showed somewhat narrower resonances than the experiment. However, the large contrast was described well, and even the agreement between experiment and theory for the broad structure was better than in the case of the small bright resonances observed under linear excitation. Again, the model's idealization of the laser beam profile should be kept in mind.

V. CONCLUSION

Nonlinear magneto-optical resonances in the hyperfine transitions of the D_2 line of atomic rubidium have been studied under excitation by a single laser field. When the exciting laser radiation was linearly polarized, bright resonances were observed at the $F_g = 2 \longrightarrow F_e = 3$ transition of ^{87}Rb and at the $F_g = 3 \longrightarrow F_e = 4$ transition of ^{85}Rb when the laser power density was very low. However, as the laser power density was increased above 0.6 mW/cm^2 or 0.8 mW/cm^2, respectively, these bright resonances became dark. The effect was described by a theoretical model based on the optical Bloch equations, which took into account all nearby hyperfine transitions, the mixing of magnetic sublevels in the external magnetic field, the coherence properties of the laser radiation, and the Doppler broadening. The parameter values in the model that could not be measured precisely were adjusted once for the entire set of measurements. These parameters were the coefficient that relates transit relaxation rate to the laser beam diameter, the coefficient that relates laser power density to the squared Rabi frequency, and the laser linewidth. The possibility of examining the density matrix calculated for the precise system under study provided useful insight into the role of competing effects that take place in the experiment.

In the case of circularly polarized excitation of the $F_g = 2 \longrightarrow F_e = 3$ transition of ^{87}Rb, a bright resonance was observed at room temperature, but this bright resonance became dark as the vapor temperature was increased. The change might be related to reabsorption effects.

The ability of the model to describe subtle effects, such as the change from bright to dark resonances in a system whose hyperfine structure was not resolved under Doppler broadening confirmed that the model is an adequate tool for studying nonlinear magneto-optical resonances in spite of its simplifying assumptions about the transit relaxation time and the laser power density distribution. In order to test its utility in understanding other systems, the model was applied retrospectively to previously published results in which a simpler theory failed to describe the measured results. In that case (see Ref. [32], Fig. 3a), a broad dark resonance was measured at low power on the the $F_g = 3 \longrightarrow F_e = 3,4,5$ transition of cesium excited with linearly polarized light, but the theory, which included only the cycling transition, predicted a narrow bright resonance. Our model was able to show the correct sign and width of the resonance, which underlines the need for detailed theoretical treatments. Work is currently in progress to apply the model to describing nonzero resonance signals (see, for example, Ref. [33]) and nonlinear magneto-optical resonances for D_2 excitation in a rubidium vapor cell with a width of several hundred nanometers (see, for example, Ref. [34]). However, the ability to change a bright resonance into a dark resonance by increasing the temperature suggests that, in the future, reabsorption effects should be included in the model.

ACKNOWLEDGMENTS

We thank Andrey Jarmola for helpful advice and discussions. We gratefully acknowledge support from the Latvian State Research Programme Grant No. 2010/10-4/VPP-2/1, ERAF project no. 2DP/2.1.1.1.0/10/APIA/VIAA/036, and ESF project no. 2009/0223/1DP/1.1.1.2.0./09/APIA/VIAA/008.

[1] E. Arimondo, in *Progress in Optics*, edited by E. Wolf, Vol. 35 (Elsevier, Amsterdam, 1996), pp. 257–354 [http://www.sciencedirect.com/science/article/pii/S0079663808705316].

[2] P. R. Hemmer, A. V. Turukhin, M. S. Shahriar, and J. A. Musser, Opt. Lett. **26**, 361 (2001).

[3] W. R. Kelly, Z. Dutton, J. Schlafer, B. Mookerji, T. A. Ohki, J. S. Kline, and D. P. Pappas, Phys. Rev. Lett. **104**, 163601 (2010).

[4] S. E. Harris, J. E. Field, and A. Imamoglu, Phys. Rev. Lett. **64**, 1107 (1990).

[5] M. Fleischhauer, A. Imamoglu, and J. P. Marangos, Rev. Mod. Phys. **77**, 633 (2005).
[6] D. Budker, W. Gawlik, D. F. Kimball, S. M. Rochester, V. V. Yashchuk, and A. Weis, Rev. Mod. Phys. **74**, 1153 (2002).
[7] A. M. Akulshin, S. Barreiro, and A. Lezama, Phys. Rev. A **57**, 2996 (1998).
[8] Y. Dancheva, G. Alzetta, S. Cartalava, M. Taslakov, and C. Andreeva, Opt. Commun. **178**, 103 (2000).
[9] D. V. Brazhnikov, A. V. Taichenachev, A. M. Tumaikin, V. I. Yudin, I. I. Ryabtsev, and V. M. Entin, JETP Lett. **91**, 625 (2010).
[10] H. H. Kim, M. H. Ahn, K. Kim, J. B. Kim, and H. S. Moon, J. Korean Phys. Soc. **46**, 1109 (2005).
[11] K. Dahl, L. S. Molella, R.-H. Rinkleff, and K. Danzmann, Opt. Lett. **33**, 983 (2008).
[12] A. A. Zhukov, S. A. Zibrov, G. V. Romanov, Y. O. Dudin, V. V. Vassiliev, V. L. Velichansky, and V. P. Yakovlev, Phys. Rev. A **80**, 033830 (2009).
[13] N. Ram and M. Pattabiraman, J. Phys. B **43**, 245503 (2010).
[14] L. S. Molella, K. Dahl, R.-H. Rinkleff, and K. Danzmann, Opt. Commun. **282**, 3481 (2009).
[15] J. C. Lehmann and C. Cohen-Tannoudji, C. R. Acad. Sci. (Paris) **258**, 4463 (1964).
[16] F. Renzoni, S. Cartaleva, G. Alzetta, and E. Arimondo, Phys. Rev. A **63**, 065401 (2001).
[17] J. Alnis and M. Auzinsh, Phys. Rev. A **63**, 023407 (2001).
[18] J. L. Picqué, J. Phys. B **11**, L59 (1978).
[19] C. Andreeva, S. Cartaleva, Y. Dancheva, V. Biancalana, A. Burchianti, C. Marinelli, E. Mariotti, L. Moi, and K. Nasyrov, Phys. Rev. A **66**, 012502 (2002).
[20] Y. P. Malakyan, S. M. Rochester, D. Budker, D. F. Kimball, and V. V. Yashchuk, Phys. Rev. A **69**, 013817 (2004).
[21] K. Blushs and M. Auzinsh, Phys. Rev. A **69**, 063806 (2004).
[22] M. Auzinsh, R. Ferber, F. Gahbauer, A. Jarmola, and L. Kalvans, Phys. Rev. A **78**, 013417 (2008).
[23] M. Auzinsh, R. Ferber, F. Gahbauer, A. Jarmola, and L. Kalvans, Phys. Rev. A **79**, 053404 (2009).
[24] S. Stenholm, *Foundations of Laser Spectroscopy* (Dover, Mineoloa, NY, 2005).
[25] D. A. Steck, *Rubidium 85 d line data* (Sep. 2009; revision 2.1.2, 12 August 2009) [http://steck.us/alkalidata].
[26] L. Allen and J. H. Eberly, *Optical Resonance and Two Level Atoms* (Wiley, New York, 1975).
[27] N. G. van Kampen, Phys. Rep. **24**, 171 (1976).
[28] M. Auzinsh, D. Budker, and S. M. Rochester, Phys. Rev. A **80**, 053406 (2009).
[29] D. A. Steck, *Rubidium 87 d line data* (Aug. 2009; revision 2.1.2, 12 August 2009) [http://steck.us/alkalidata].
[30] A. B. Matsko, I. Novikova, and G. R. Welch, J. Mod. Opt. **49**, 367 (2002).
[31] S. Gozzini, L. Marmugi, D. Slavov, A. Lucchesini, and S. Cartaleva, Proc. SPIE **7747**, 77470O (2011).
[32] A. V. Papoyan, M. Auzinsh, and K. Bergmann, Eur. Phys. J. D **21**, 63 (2002).
[33] J. Alnis, K. Blushs, M. Auzinsh, S. Kennedy, N. Shafer-Ray, and E. Abraham, J. Phys. B **36**, 1161 (2003).
[34] M. Auzinsh, R. Ferber, F. Gahbauer, A. Jarmola, L. Kalvans, A. Papoyan, and D. Sarkisyan, Phys. Rev. A **81**, 033408 (2010).